Geochemistry, Geophysics, Geosystems

RESEARCH ARTICLE
10.1029/2018GC007697

Dating Clinopyroxene Phenocrysts in Submarine Basalts Using $^{40}Ar/^{39}Ar$ Geochronology

Kevin Konrad[1], Anthony A. P. Koppers[1], Andrea M. Balbas[1,2], Daniel P. Miggins[1], and Daniel E. Heaton[1]

[1]College of Earth, Ocean, and Atmospheric Science, Oregon State University, Corvallis, OR, USA, [2]Department of Geological and Planetary Sciences, California Institute of Technology, Pasadena, CA, USA

Key Points:
- Clinopyroxene phenocrysts are a viable phase for $^{40}Ar/^{39}Ar$ age determinations
- The elevated proxy K/Ca values indicate some other phase(s) within the clinopyroxene crystals are hosting the K
- Silicate melt trapped along grain defects or secondary melt inclusion bands are the most likely K- and $^{40}Ar^*$-bearing phases

Supporting Information:
- Supporting Information S1

Correspondence to:
K. Konrad,
konradke@oregonstate.edu

Citation:
Konrad, K., Koppers, A. A. P., Balbas, A. M., Miggins, D. P., & Heaton, D. E. (2019). Dating clinopyroxene phenocrysts in submarine basalts using $^{40}Ar/^{39}Ar$ geochronology. *Geochemistry, Geophysics, Geosystems*, *20*, 1041–1053. https://doi.org/10.1029/2018GC007697

Received 18 MAY 2018
Accepted 13 JAN 2019
Accepted article online 28 JAN 2019
Published online 18 FEB 2019

Abstract Dating submarine basalts using $^{40}Ar/^{39}Ar$ geochronology is often hindered by a lack of potassium-bearing phenocrystic phases and severe alteration in the groundmass. Clinopyroxene is a common phenocrystic phase in seafloor basalts and is highly resistive to low-temperature alteration. Here we show that clinopyroxene phenocrysts separated from marine basalts are a viable phase for $^{40}Ar/^{39}Ar$ incremental heating age determinations. We provide results from a pilot study comprising 16 age experiments from nine clinopyroxene separates, five of which from samples with dated coeval phases. The clinopyroxene ages range from 11.5 to 112 Ma with relatively high uncertainties (ranging from 0.8% to 7.1%; median of 1.9%) compared to more traditional phases. The clinopyroxene age plateaus form at low to moderate temperature steps and are characterized by relatively elevated K/Ca of 0.002–0.4, suggesting that other K-bearing phases hosted within the clinopyroxene are likely degassing to yield the $^{40}Ar/^{39}Ar$ age information. There are three possible origins for the K and corresponding $^{40}Ar^*$ including films of trapped melt/nanomineral inclusions along grain defects, secondary melt inclusion bands, or variations in degassing behaviors between lower and higher crystalline Ca pyroxene phases. Regardless of the source of the K, the age determinations are successful with 75% of the experiments producing long plateaus (>60% ^{39}Ar released) with mean square of the weighted deviations ranging from 0.6 to 1.5 and probability of fit values >0.05. We conclude that clinopyroxene dating by the $^{40}Ar/^{39}Ar$ method has the potential to provide a wealth of information for previously undated, altered seafloor lithologies and continental equivalents.

1. Introduction

The ability to provide $^{40}Ar/^{39}Ar$ age determinations for basaltic lava flows is often limited by the degree of alteration and an absence of potassium-bearing phenocrystic mineral phases, especially in submarine basalts. Samples recovered from the ocean basins by dredges, scientific ocean drilling, or remote vehicle dives are often heavily altered and unable to be dated by traditional geochronological techniques. Experience has shown that only a minority of the collected submarine lavas can be dated, if they contain unaltered plagioclase, hornblende, or biotite phenocrysts, or if they contain holocrystalline groundmass that can be cleaned up by applying acid leaching protocols (e.g., Konrad et al., 2018; Koppers et al., 2000, 2003). Clinopyroxene, the most common phenocryst phase in alkaline basalts, is highly resistive to weathering by prolonged exposure to seawater (Bach et al., 2004; Staudigel et al., 1996). However, phenocrystic clinopyroxene previously has not been significantly sought out as a datable mineral phase since K is highly incompatible in the crystal structure (Hart & Dunn, 1993) and thus results in the crystallization of ultralow potassium clinopyroxene. Recent work on ancient metamorphic clinopyroxene (Burgess et al., 1992), a single alkaline basalt (Konrad et al., 2018), dolerites in terrestrial large igneous provinces (Ware & Jourdan, 2018), and a plagiogranite (Zhong et al., 2018) indicate that age determinations are obtainable. In addition, diffusion experiments show that argon is highly retentive in clinopyroxene, with closure temperatures of 600 to 800 °C (Cassata et al., 2010, 2011; Kunz et al., 1997) making clinopyroxene a viable phase for thermochronology studies and applications in high-grade metamorphic rocks (Ware & Jourdan, 2018).

Here we show in a pilot study that augitic clinopyroxenes separated from marine alkaline basalts provide useable $^{40}Ar/^{39}Ar$ age determinations when measured on modern multicollector mass spectrometers. However, the primary K and associated radiogenic $^{40}Ar^*$ appears to potentially reside within a hosted phase, not the augite host mineral, and is released throughout the low to moderate temperature steps in

incremental heating experiments. We also show that intercrystalline held argon only begins to release at the highest temperature steps and that samples containing rare primary melt inclusions produce (small) pulses of excess radiogenic ^{40}Ar that do not typically compromise the heating spectra. Dating clinopyroxene in alkaline submarine basalts opens up a new avenue in the geochronology of dredge and scientific ocean drilling (DSDP, ODP and IODP) samples. It has the potential to contribute significantly to our understanding of all submarine volcanism, including the formation of seamounts, large igneous provinces, and island arcs, with implications for plate tectonics, subduction zone processes, mantle convection, and plume motions.

2. Methods

2.1. Sample Suite

The nine basalt samples used in this study come from seamounts in the Western Pacific Seamount Province (samples NWO-1, HIM-3, MAL-2, and JEN-4; Koppers et al., 2003; Figure 1), the Tuvalu seamount chain that is an older extension of the Rurutu hot spot (samples RR1310-D7-09, -D13-01, -D2104; Finlayson et al., 2018; Konrad et al., 2018), and from the International Ocean Discovery Program drill cores in the Izu-Bonin-Mariana (IBM) forearc (samples 352-U1439C-2R-3W, 29-32 and 352-U1442A-15R-1W, 61-64; Reagan et al., 2019). The seamount samples are seawater altered alkaline basalts and were primarily chosen due to the availability of robust $^{40}Ar/^{39}Ar$ age constraints from other K-bearing phenocrystic phases, such as plagioclase, hornblende, and biotite, or other basalts from the dredge/core. The IBM samples consist of a forearc basalt with holocrystalline groundmass (352-U1442A-15R-1W, 61–64) and a glassy boninite (352-U1439C-2R-3W, 29-32). The two IBM samples are relatively unaltered and contain fresh clinopyroxene as the only phenocrystic phase. All clinopyroxene appear to be augite or titino-augite that are either green (RR1310-D07-09, MAL-2, and the IBM samples) or brown to black in color (all other separates). The MAL-2 sample had two types of augite pyroxenes, and both green and brown pyroxene separates were prepared. There are currently no constraints on the proportion of pigeonite (low-Ca clinopyroxene) to augite (high-Ca clinopyroxene) for the analyzed mineral separates. Despite the altered nature of the basalts, the clinopyroxene phenocrysts are typically fresh based on petrographic examinations, with the exception of sample HIM-3, which is severely altered (Figure 1b).

2.2. Sample Preparation

Clinopyroxene was separated from basalts by crushing and sieving the rock to grain size fractions of 350–250 μm. These fractions were washed in deionized water and dried in a 50 °C oven overnight, prior to clinopyroxene being concentrated using a Frantz magnetic separator. Concentrated separates were then subjugated to sequential 1-hr sonicated baths in 3N HCl, 6N HCl, 1N HNO_3, and 3N HNO_3 interspersed with thorough rinsing steps and followed by sonication in ultrapure water. This acid leaching protocol was developed to remove any adhering secondary clays and carbonate grains from the mineral separate (Koppers et al., 2000). Samples were dried overnight in a 50 °C oven prior to being handpicked under a binocular microscope, focusing on achieving homogeneous and pure clinopyroxene separates. Approximately 70–80 mg of clinopyroxene for each lava flow was packed into aluminum capsules for irradiation. Fish Canyon Tuff sanidine was used as a fluence monitor, loaded at the bottom, top, and between every three sample packets. The sample columns were then irradiated for 6 hr in the CLICIT position of the Oregon State University's TRIGA reactor.

2.3. $^{40}Ar/^{39}Ar$ Analysis

For each incremental heating experiment approximately 40 mg (out of the total 80 mg) clinopyroxene was loaded onto copper trays and brought under vacuum to be analyzed on one of the two ARGUS-VI mass spectrometers of the OSU Argon Geochronology Laboratory (http://geochronology.coas.oregonstate.edu). The second 40-mg split was analyzed in a separate experiment to test for reproducibility of the resulting incremental heating age spectra. To remove atmospheric argon adhering to the grain surfaces, samples were "precleaned" at low CO_2 laser intensities (0.8–1.4%) with the gasses being pumped immediately without measurement. The clinopyroxene samples were then subjected to 14 to 23 incrementally increasing heating steps, with blanks run prior to, after, and between every two heating steps, totaling 8 to 12 blanks for each experiment. Extracted gas was exposed to a series of getters held at 400 °C (ST101), 200 °C (ST172), and room temperature (ST172, AP10) for a total of 3 min. The cleaned gas was then inlet into one of the

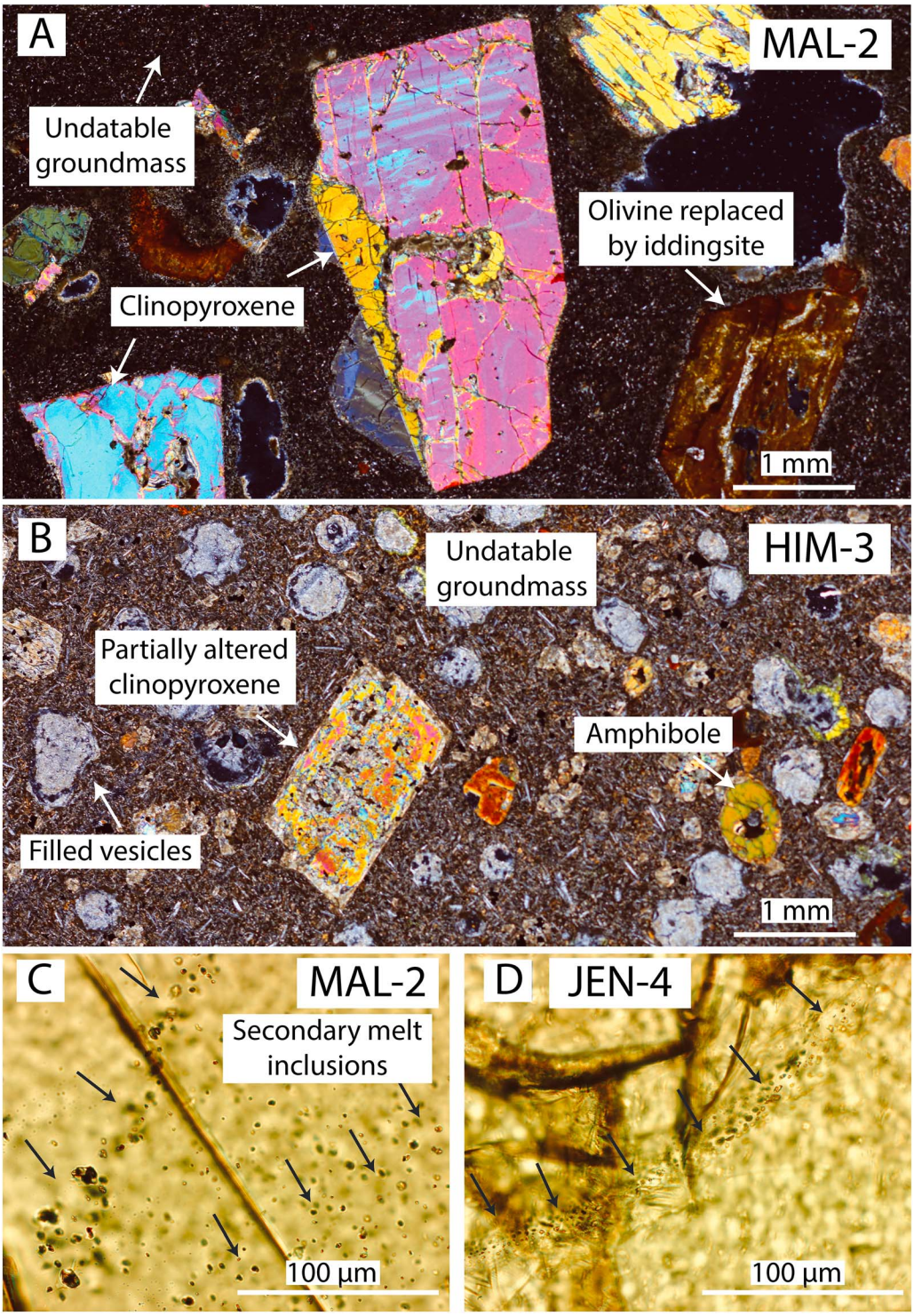

Figure 1. Petrographic images of samples used in this study. (a) A cross-polarized image of sample MAL-2. (b) A cross-polarized image of sample HIM-3; note the degradation of clinopyroxene in this sample. (c) Curvilinear secondary melt inclusion bands in a clinopyroxene from MAL-2. Arrows indicate the direction the bands traverse into the crystal. (d) A secondary melt inclusion band from sample JEN-4.

Table 1
$^{40}Ar/^{39}Ar$ Age Determinations for Clinopyroxene Experiments

Sample information					Plateau									
Sample name	Material	Location	Latitude (degree)	Longitude (degree)	Age (Ma)	±2σ (i, Ma)	±2σ (f, Ma)	^{39}Ar	K/Ca	±2σ	MSWD	*P* (%)	*n*	*N*
Western Pacific Seamount Province														
NWO-1	CPX	North-Wod-En, WPSP	15.97	162.93	N/A									23
HIM-3a	CPX	Himu Seamount, WPSP	21.70	151.70	N/A									23
HIM-3b	CPX				N/A									23
MAL-2 BROWN	CPX	Maloney, WPSP	21.05	157.15	**98.76**	**1.10**	2.46	81%	0.03	0.013	1.07	38%	14	23
MAL-2 GREEN	CPX				**100.18**	**1.17**	2.52	65%	0.389	0.054	1.00	44%	9	23
MAL-2 Stack (n = 2)					**99.40**	**0.85**	2.37	73%	0.03	0.011	1.15	29%	23	46
JEN-4a	CPX	Jennings, WPSP	20.87	156.17	**112.96**	**1.44**	2.89	88%	0.199	0.059	1.03	42%	17	23
JEN-4b	CPX				**111.41**	**1.85**	3.09	87%	0.009	0.002	1.06	39%	19	23
JEN-4 Stack (n = 2)	CPX				**112.37**	**1.16**	2.75	87%	0.009	0.004	1.07	36%	36	46
Tuvalu Seamount Chain														
RR1310-D21-04a	CPX	Nukulaelae, Tuvalu Seamounts	−9.30	179.67	12.07	0.91	0.95	93%	0.019	0.011	0.68	81%	16	23
RR1310-D21-04b	CPX				14.67	2.62	2.64	100%	0.001	0.001	1.24	23%	16	23
RR1310-D21-04 Stack (n = 2)	CPX				12.41	0.88	0.92	95%	0.002	0.003	1.06	37%	32	46
RR1310-D07-09a	CPX	Tefolaha, Tuvalu Seamounts	−5.97	176.96	**49.34**	**2.48**	2.72	71%	0.07	0.008	0.9	50%	7	14
RR1310-D07-09b	CPX				**46.53**	**2.10**	2.35	67%	0.07	0.007	1.48	13%	12	22
RR1310-D07-09c	CPX				**49.33**	**1.60**	1.94	79%	0.031	0.012	0.48	94%	14	23
RR1310-D07-09 Stack (n = 3)	CPX				**48.28**	**1.10**	1.54	72%	0.043	0.009	1.08	35%	33	59
RR1310-D13-01a	CPX	Tayasa, Tuvalu Seamounts	−8.62	177.91	**47.43**	**2.94**	3.13	82%	0.026	0.009	1.39	15%	15	23
RR1310-D13-01b	CPX				N/A									23
IBM Forearc														
352-U1439C-2R-3W 29-32	CPX	IBM Forearc	28.41	142.61	**50.33**	**0.55**	1.25	84%	0.097	0.019	1	43%	9	17
352-U1442A-15R-1W 61-64	CPX	IBM Forearc	28.41	142.62	**51.02**	**0.39**	1.21	82%	0.0808	0.0032	0.55	80%	8	15

Note. i = internal uncertainties; f = full external uncertainties. MSWD = mean square of the weighted deviavations. n = heating step used in age calculation; N = total heating steps. P = Probability of Fit. SF = spreading factor. IBM = Izu-Bonin-Mariana. WPSP = Western Pacific Seamount Province. Recommended sample age and uncertainty are shown in bold. IBM forearc samples are from Reagan et al. (2019).

ThermoScientific ARGUS-VI mass spectrometers. Seven clinopyroxene were analyzed on the ARGUS-VI-D using 10^{12} Ω faraday cups for m/z 40, 39, 38, and 37 and an ion-counting CuBe electron multiplier for m/z 36. Two samples (352-U1439C-2R-3W, and 29-32 and 352-U1442A-15R-1W, 61-64) were analyzed on the ARGUS-VI-E using 10^{13} Ω faraday cups for m/z 39, 38, and 37; a 10^{12} Ω faraday cup for m/z 40; and an ion-counting CuBe electron multiplier for m/z 36. Analyses lasted for about 6.5 min (150 data points collected at 2-s integration times) with the time "0" set synchronous to the moment of gas inlet into the spectrometer and data acquisition starting after about 25 s of argon gas equilibration in the low volume (650 cm^3) ARGUS-VI.

All age determinations were calculated using ArArCALC v.2.7.0 (Koppers, 2002). For the age calculations an age of 28.201 ± 0.046 Ma (2σ) was used for the Fish Canyon Tuff fluence monitor (Kuiper et al., 2008) and a total decay constant of $5.530 \pm 0.097 \times 10^{-10}$ $year^{-1}$ (2σ; Min et al., 2000). A polynomial function was fit to blanks analyzed during the experiment, and unknown analyses were blank corrected based on time of measurement. All reported internal uncertainties (Table 1) include in addition to analytical uncertainty on the peak measurements, corrections for baselines, irradiation constants, the J value curve, collector calibrations (whereby the CuBe multiplier is cross calibrated to the nearest +1 AMU Faraday cup, using a series of low intensity air shot ^{36}Ar peak measurements), mass fractionation (calibrated against a marine air standard,

Table 1 *(continued)*

Sample information	Inverse isochron								Total fusion				
Sample name	Age (Ma)	±2σ (i, Ma)	±2σ (f, Ma)	$^{40}Ar/^{36}Ar$ intercept	±2σ	SF	MSWD	*P* (%)	Age (Ma)	±2σ (i, Ma)	±2σ (f, Ma)	K/Ca	±2σ
Western Pacific Seamount Province													
NWO-1	N/A								89.24	0.31	2.01	0.093	0.001
HIM-3a	N/A								139.84	14.09	14.43	0.078	0.004
HIM-3b	N/A								191.20	16.65	17.18	0.028	0.003
MAL-2 BROWN	98.69	1.35	2.58	296.40	4.01	63%	1.1	36%	104.33	1.23	2.63	0.135	0.003
MAL-2 GREEN	100.04	3.09	3.81	299.67	55.11	20%	1.14	34%	110.22	1.43	2.84	0.136	0.004
MAL-2 Stack ($n = 2$)	99.54	0.99	2.43	295.25	3.92	64%	1.17	27%	107.08	0.95	2.56	0.136	0.002
JEN-4a	112.62	3.16	4.03	297.97	11.96	68%	1.34	17%	110.44	1.66	2.96	0.16	0.006
JEN-4b	109.64	2.58	3.55	299.18	3.25	62%	0.84	65%	112.71	1.90	3.14	0.067	0.006
JEN-4 Stack ($n = 2$)	111.91	1.61	2.96	297.59	3.03	68%	1.14	26%	111.49	1.26	2.78	0.097	0.006
Tuvalu Seamount Chain													
RR1310-D21-04a	**13.09**	**1.31**	1.34	287.30	8.14	43%	0.41	97%	10.80	1.21	1.23	0.056	0.002
RR1310-D21-04b	**10.66**	**2.98**	2.99	302.98	3.31	9%	1.1	36%	23.33	4.07	4.11	0.006	0.001
RR1310-D21-04 Stack ($n = 2$)	**11.50**	**1.01**	1.05	301.38	2.52	40%	1.12	30%	13.60	1.24	1.28	0.02	0.001
RR1310-D07-09a	48.75	3.40	3.57	297.61	5.30	70%	0.95	45%	69.31	3.20	3.56	0.082	0.004
RR1310-D07-09b	47.69	2.74	2.94	294.02	3.28	69%	1.47	14%	46.54	1.72	2.02	0.067	0.002
RR1310-D07-09c	50.22	2.47	2.71	294.58	2.37	40%	0.68	77%	51.23	1.79	2.13	0.022	0.001
RR1310-D07-09 Stack ($n = 3$)	48.99	1.59	1.93	294.89	1.76	77%	1.14	27%	56.69	1.35	1.85	0.043	0.001
RR1310-D13-01a	49.10	3.58	3.75	294.65	3.53	52%	1.47	12%	69.38	3.50	3.83	0.042	0.002
RR1310-D13-01b	N/A								66.83	4.14	4.40	0.019	0.001
IBM Forearc													
352-U1439C-2R-3W 29-32	50.48	0.99	1.50	292.72	17.03	57%	1.13	34%	48.96	0.73	1.32	0.063	0.001
352-U1442A-15R-1W 61-64	51.07	0.49	1.25	294.78	5.36	51%	0.64	70%	49.77	0.50	1.22	0.05	0.001

assuming an $^{40}Ar/^{36}Ar$ value of 295.5), blanks, and post irradiation radioactive decay of ^{37}Ar and ^{39}Ar. External uncertainties include the internal uncertainty along with the uncertainties on the decay constant, natural element abundance ratios, and the fluence monitor age. Samples for which two or more splits of clinopyroxene have been analyzed were "stacked" with all steps in their individual age plateaus being combined into an overall weighted mean and into the isochron calculations, significantly improving the statistics on the analyzes. All previously published $^{40}Ar/^{39}Ar$ ages discussed herein are recalculated with the same fluence monitor mineral age and decay constants shown above. All age uncertainties are reported on the 2σ confidence level.

3. Results

For this study, a useable age was classified as a plateau containing >60% of the $^{39}Ar_{(k)}$ released as well as a probability of fit (*P*) value >5%. Four out the 16 individual age experiments failed to produce a plateau that met our criteria, and thus, no age determinations are reported. When multiple splits of the same basalt were analyzed, the resulting data were stacked, wherein the individual heating steps were combined into one large experiment. The clinopyroxenes in this study typically produced long age plateaus (72–95% of ^{39}Ar released, including 7–19 steps) with isochron intercepts within error of atmospheric values ($^{40}Ar/^{36}Ar = 295.5$; Table 1, Figures 2–4, and Supporting Information S1). Only one lava flow, RR131-D21-04,

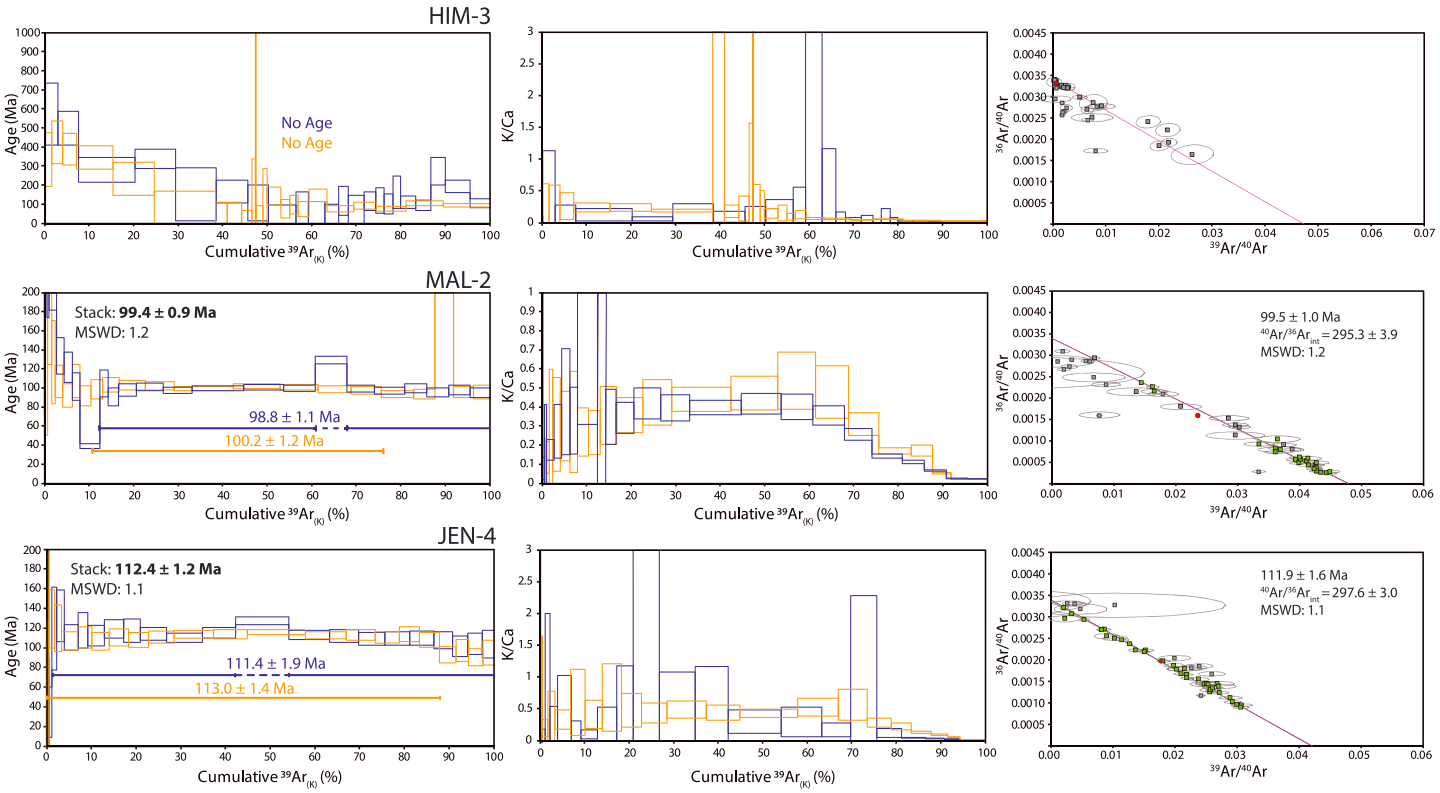

Figure 2. The $^{40}Ar/^{39}Ar$ incremental heating age spectra and inverse isochrons for clinopyroxene separates from HIM-3, MAL-2, and JEN-4. Individual experiment plateaus are color coded, and the stacked age is shown in black. Thick black lines indicate the selected plateau range with dashed segments representing steps not used in the age calculation. Inverse isochrons are shown on the right with points used in the plateau calculation shown in green with unused steps shown in gray. The red dot represents the total fusion value. The calculated isochrons are shown with a pink line, while an atmospheric reference line is shown in black. All uncertainties are displayed at the 2σ confidence level.

contained a supraatmospheric $^{40}Ar/^{36}Ar$ intercept of 301.4 ± 2.5, which may indicate the possibility of excess radiogenic ^{40}Ar trapped in the clinopyroxenes. In that one case, the inverse isochron age of 11.5 ± 1.0 Ma was preferred. For all other samples, the plateau ages are preferred and reported here (Table 1). Spreading factors (Jourdan et al., 2009) for isochrons are typically excellent, ranging from 40% to 77%. Mean square of the weighted deviations (MSWD) values for the clinopyroxene experiments range from 0.6 to 1.4 (median of 1.1) and indicate that the data scatter across the age plateaus is in line with the measured levels of analytical uncertainty in the individual incremental heating steps. *P* values range from 15% to 80% for the successful age determinations. For sample MAL-2, both green (100.18 ± 1.17 Ma) and brown (98.76 ± 1.1 Ma) clinopyroxene separates were analyzed with no discernable difference observed between the splits. Samples occasionally display a single heating step with a significant increase in apparent age (e.g., MAL-2 and JEN-4). These discordant steps show evidence for excess ^{40}Ar in the isochron plots and thus are not included in the plateau age calculations (dashed line segments; Figures 1–3). These observations are inherent to the presence of (micro) mineral and melt inclusions in the clinopyroxene and are discussed in detail further below.

Individual incremental heating steps for the clinopyroxenes yielded relatively large age uncertainties, resulting in weighted mean plateau ages with 2σ uncertainties ranging from 0.8% to 17.9% (median of 1.9%) for the stacked experiments. This is to be expected because clinopyroxenes in alkaline basalts have extremely low potassium concentrations (K_2O < 0.01 wt. %) while being abundant in calcium (CaO >20.00 wt. %; Hart & Dunn, 1993; Miyazaki et al., 2018; Nisbet & Pearce, 1977). However, we observed that the higher uncertainties are due to two reasons, namely, difficulty in measuring low 39 and 37 mass peaks, which are primarily sourced from irradiated K and Ca, respectively. The situation improved by measuring m/z 37, 38, and 39 for samples 352-U1439C-2R-3W, 29-32 (50.33 ± 0.55 Ma) and 352-U1442A-15R-1W, 61-64 (51.02 ± 0.39 Ma)

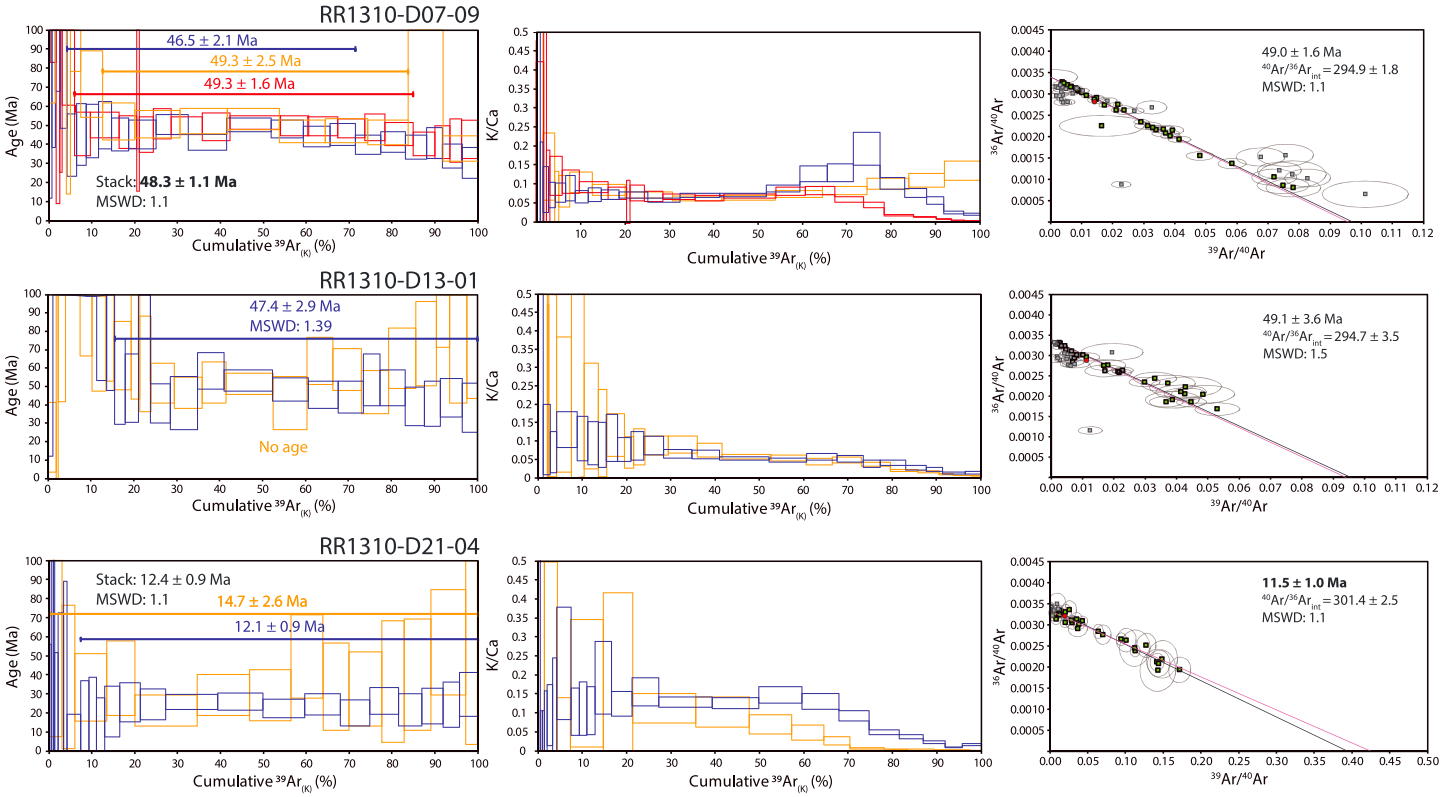

Figure 3. $^{40}Ar/^{39}Ar$ incremental heating age spectra and inverse isochrons for clinopyroxene separates from RR1310-D07-09, RR1310-D13-01, and RR1310-D2104. All parameters are the same as in Figure 2. The preferred inverse isochron age is shown in bold for RR1310-D21-04.

with 10^{13} Ω faraday cups on the ARGUS-VI-E, which allows for more robust measurements at low intensities due to a significantly reduced baseline noise (by a factor of ~2.5) compared to the 10^{12} Ω faraday cups on ARGUS-VI-D. Importantly, the overall low intensities in the ^{37}Ar measurements seem to indicate that little of the primary Ca-derived argon in the clinopyroxene crystalline matrix is being degassed at the temperature steps that were applied during most of the incremental heating, except maybe at the highest temperatures at the end of each experiment.

This effect also is seen in the K/Ca ratios that provide a key compositional signature for the sample domain degassing at each individual heating step, calculated as the ratio between measured $^{39}Ar_{(K)}$ and $^{37}Ar_{(Ca)}$ components. In our experiments, the K/Ca for clinopyroxene yields average values ranging from 0.001 to 0.4 (median of 0.03) for the steps included in the age plateau calculations (Table 1 and Figure 5). These values are significantly elevated compared to average spot analyses of alkaline basalt clinopyroxene (K/Ca < 0.0001; Koppers et al., 2000; Miyazaki et al., 2018; Nisbet & Pearce, 1977) using electron microprobes, again indicating that some other phase(s) than clinopyroxene are primarily outgassing radiogenic $^{40}Ar^*$ during the incremental heating experiments. Interestingly, the K/Ca values typically decrease extremely rapidly at the highest temperatures and approach expected low clinopyroxene values, which is caused by a large pulse in $^{37}Ar_{(Ca)}$ being released, most likely from the clinopyroxene itself (Figure 5). This pulse is significant as between 50% and 70% of the total amount of $^{37}Ar_{(Ca)}$ for a given clinopyroxene is degassed in just the final 20%–30% of the experiments. Occasionally, some of the moderate to high-temperature heating steps produce significant increases in K/Ca, likely indicating rapid degassing of a high K/Ca phase within the clinopyroxene crystals (e.g., RR1310-D07-09). These observations are key in interpreting the clinopyroxene age spectra in terms of which degassing domains are responsible for creating the wide age plateaus, pointing to a major role for preferential degassing of mineral and/or melt inclusions and a diminished role for the primary magmatic clinopyroxene host crystals, contrary to the findings of Ware and Jourdan (2018) for dolerite clinopyroxenes in terrestrial large igneous provinces.

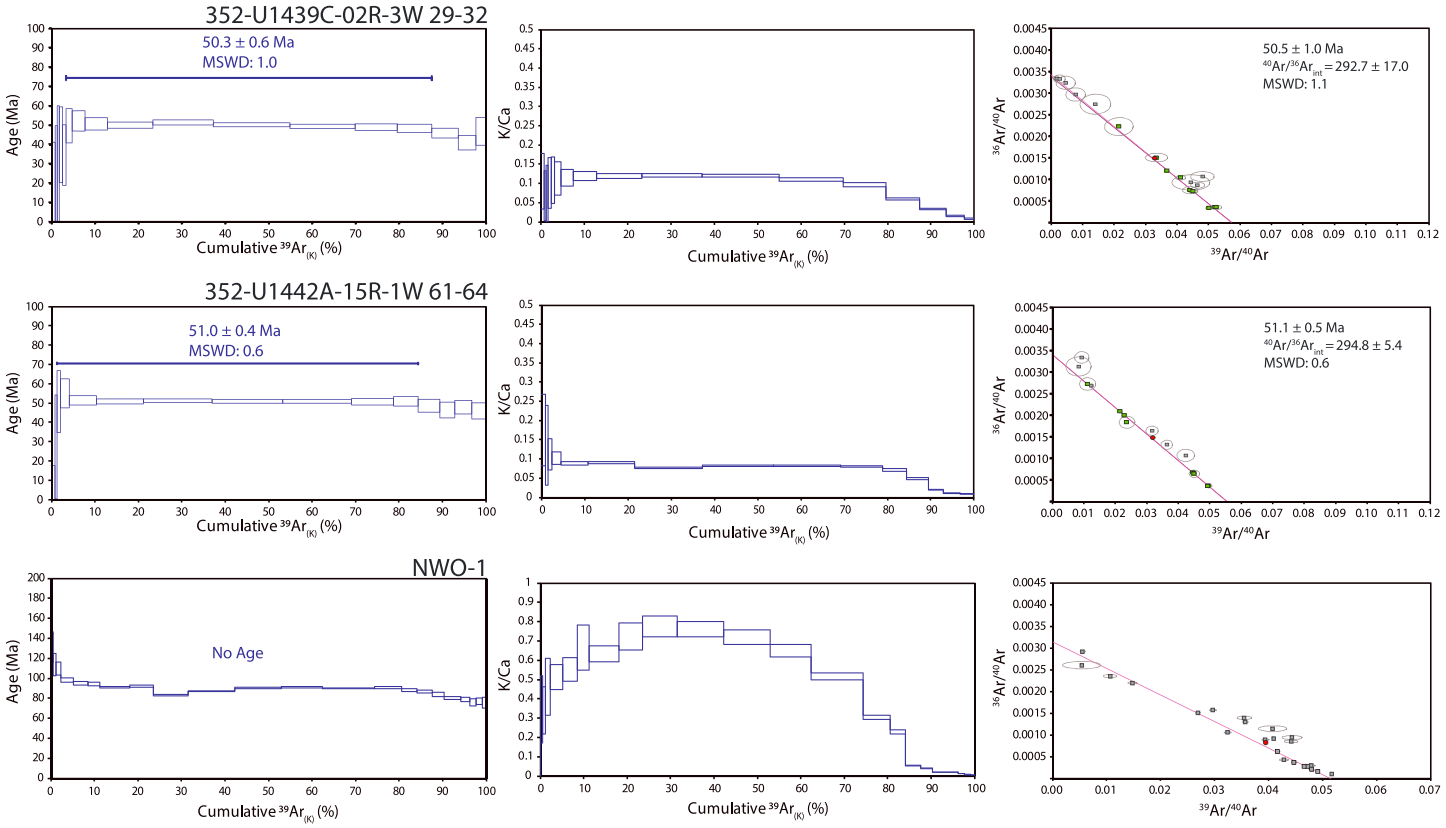

Figure 4. The $^{40}Ar/^{39}Ar$ heating spectrums and inverse isochrons for clinopyroxene separates from 352-U1439C-02R-3W, 20-32; 352-U1442A-15R-1W, 61-64 (Reagan et al., 2019); and NWO-1. All parameters are the same as in Figure 2.

4. Discussion

4.1. Reliability of Clinopyroxene Ages

The simplest means of determining the reliability of clinopyroxene $^{40}Ar/^{39}Ar$ age determinations is to compare the ages to coeval mineral phases. We have direct age comparisons for five of the clinopyroxene samples analyzed (Figure 6). These include concordant samples RR1310-D13-01 (clinopyroxene = 47.4 ± 2.9; plagioclase = 50.5 ± 0.2 Ma; Konrad et al., 2018) and MAL-2 (clinopyroxene = 99.4 ± 0.9; groundmass = 99.7 ± 0.6 Ma; Koppers et al., 2003). Two separates are similar but 5% to 6% older or younger than the coeval phase. These samples are RR1310-D07-09 (clinopyroxene = 48.3 ± 1.1; plagioclase = 51.0 ± 0.4 Ma; Konrad et al., 2018) and JEN-4 (clinopyroxene = 112.4 ± 1.2; groundmass = 105.7 ± 0.6 Ma; Koppers et al., 2003). It is important to note that the clinopyroxene experiments produced higher-quality plateaus than the coeval phases, with the groundmass analyses from JEN-4 containing a MSWD of 25 (Koppers et al., 2003) and the plagioclase separate from RR1310-D07-09 displaying a MSWD of 2.6 (Konrad et al., 2018). Sample NWO-1 did not provide a reliable plateau and thus could not be compared to the coeval plagioclase separate (87.2 ± 1.0 Ma; Koppers et al., 2003), however, the total fusion results (89.2 ± 0.3 Ma) fall generally within the expected age range.

The Himu Seamount sample HIM-3 is the most significant outlier in our data set. It contains the most altered clinopyroxene grains, with significant zoning and internal degradation following its cleavage planes (Figure 1b). The plateau for both HIM-3 clinopyroxene experiments was highly disturbed and are characterized by low radiogenic $^{40}Ar^*$ yields, typically less than 10% of the total ^{40}Ar signal at each heating step. Thus, no reliable age plateau or isochron could be derived from this sample.

Samples RR1310-D21-04; HIM-3; 352-U1439C-2R-3W, 29-32; and 352-U1142A-15R-1W, 61-64 did not analyze coeval phases, or the $^{40}Ar/^{39}Ar$ dates in those cases are less reliable. However, these volcanic centers/drill cores have numerous dated lava flows. Holocrystalline basalts were analyzed from RR1310-

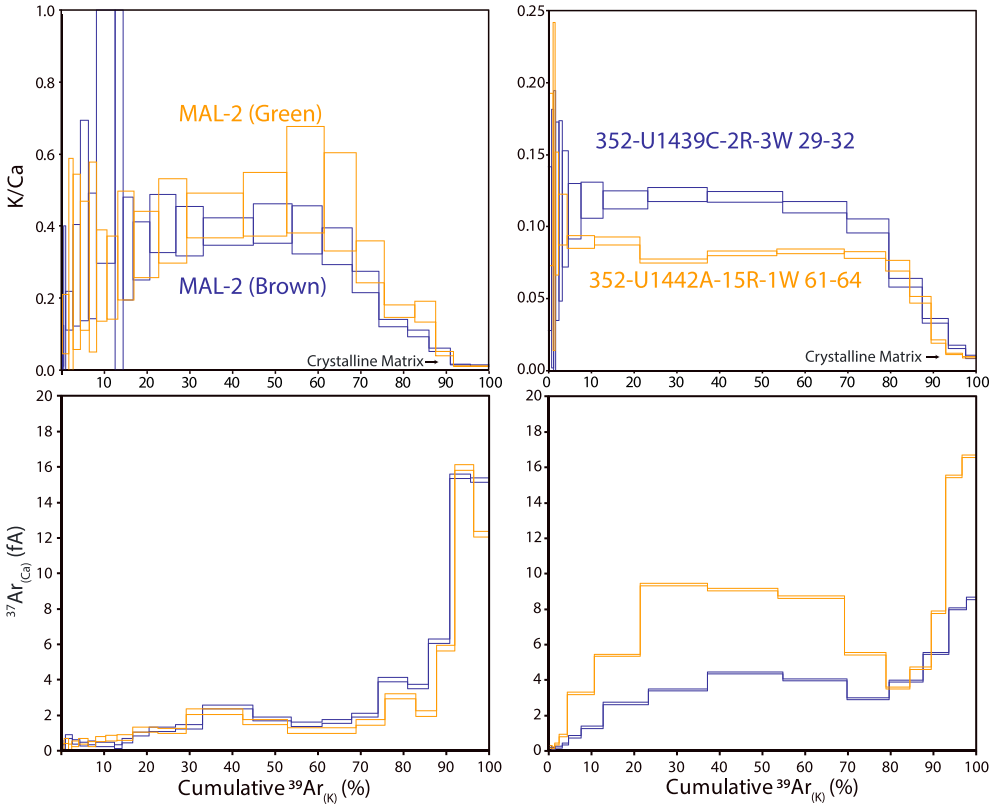

Figure 5. The K/Ca and $^{37}Ar_{(Ca)}$ variability as a function of cumulative percent $^{39}Ar_{(K)}$ released for select clinopyroxene separates.

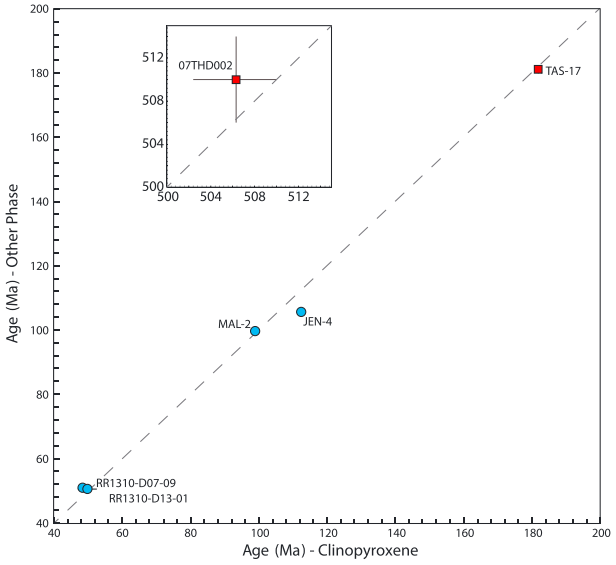

Figure 6. A one-to-one comparison of $^{40}Ar/^{39}Ar$ age determinations from clinopyroxene and the selected coeval phase. A dashed 1:1 sloped line is shown for reference. Age determinations are from this study, Koppers et al. (2003), and Konrad et al. (2018) (blue circles) and from Ware and Jourdan (2018; red square). The inset shows the continuation of the plot at 500–515 Ma to include sample 07THD002 (Jourdan et al., 2014; Ware & Jourdan, 2018).

D21 (Nukulaelae seamount) that range from 10.42 to 8.6 Ma in age (Finlayson et al., 2018), making the RR1310-D21-04 clinopyroxene age of 11.5 ± 1.0 Ma reasonable for the volcano, which could last for >7 Myr (e.g., Konter et al., 2009). Drill core recovered samples from the Izu-Bonin forearc 352-U1439C-2R-3W, 29-32 (50.3 ± 0.6 Ma) and 352-U1142A-15R-1W, 61-64 (51.0 ± 0.4 Ma) are within the expected age range for this geologic feature (55–45 Ma; Reagan et al., 2019). Overall, 75% of the clinopyroxene experiments were successful, supporting recent work arguing that this mineral phase is suitable for $^{40}Ar/^{39}Ar$ age determinations (Ware & Jourdan, 2018).

4.2. Storage Sites for Potassium and Argon Within Clinopyroxene

A key discovery of this work is that measurable quantities of $^{39}Ar_{(K)}$ and radiogenic ^{40}Ar ($^{40}Ar^*$) are released during relatively low temperature heating (<1400 °C) of phenocrystic clinopyroxene in marine and forearc lava basalts. This is accompanied by typically low $^{37}Ar_{(Ca)}$ intensities and results in elevated K/Ca ratios of 0.002–0.4 (Figure 5). Because alkaline basalt clinopyroxene has a K/Ca value of <0.0001 (Hart & Dunn, 1993; Miyazaki et al., 2018; Nisbet & Pearce, 1977), this indicates that the clinopyroxene incremental heating experiments do not begin to release abundant $^{37}Ar_{(Ca)}$ from the crystal lattice until the highest laser power settings are reached (Figure 5). This release pattern stands in contrast to the results from dolerites analyzed in Ware and Jourdan (2018) where the K/Ca values begin to decline rapidly after the first ~30% of spectra. Ware and Jourdan (2018) interpreted the K/Ca release patterns to

represent the early degassing of pigeonite (low-Ca pyroxene) followed by the higher-temperature degassing of augite (high-Ca pyroxene). In this study there is a lack of constraints on the mineral chemical compositions for the clinopyroxenes and thus we cannot fully rule out that differential pigeonite/augite degassing is controlling our K/Ca results. However, according to the degassing models of Ware and Jourdan (2018) and the activation energies (381 kJ/mol) and diffusion coefficients of Ar (1.8 cm^2/s) in diopside clinopyroxene (Cassata et al., 2010), argon should not begin degassing until the highest-temperature laser steps (>1000 °C). In addition, the relatively elevated K/Ca from the preferential degassing of pigeonite over augite should occur over a relatively small low temperature range and fails to explain how K/Ca remains elevated for up to 70% of the ^{39}Ar released in our experiments. Given the theoretical difficulty of degassing clinopyroxene at low temperatures, the $^{40}Ar/^{39}Ar$ age determinations presented herein therefore are likely not directly from the clinopyroxene crystal structure but from a more fusible phase hosted within the crystal, preferentially outgassing at lower temperatures. Mineral, fluid, and primary and secondary melt inclusions/films are the most likely candidates for hosting K and $^{40}Ar^*$ within the clinopyroxene crystals, and each type will be discussed next.

Mineral inclusions of spinel oxide are commonly observed in clinopyroxene, but because of their ultralow or void potassium contents, these inclusions are not important components in the $^{40}Ar/^{39}Ar$ experiments. Sample RR1310-D07-09 contained some plagioclase chadacrysts; however, these were avoided when the separate was handpicked. Sample RR1310-D13-01 had plagioclase phenocrysts as well as clinopyroxene, with plagioclase avoided during sample preparation. In both these samples, any potential (micro) plagioclase inclusions were unlikely the source for the $^{40}Ar^*$ as the independently measured plagioclase K/Ca is too low (D07-09 = 0.005 and D13-01 = 0.019; Konrad et al., 2018). The remaining samples analyzed in this study do not have plagioclase as a micro/phenocrystic phase. Therefore, it is likely that mineral inclusions are either not abundant or absent in this sample set and therefore not the source of $^{40}Ar^*$.

Fluid inclusions can be found in phenocrystic clinopyroxene and olivine within basalts. The fluid inclusions most commonly occur as large bands that run the length of a reannealed crystal defect (Roedder & Ribbe, 1984) and are also visible in the clinopyroxene analyzed here (Figures 1c and 1d). If initially derived from seawater, these fluid inclusions have the potential to contain a strong atmospheric contribution with a $^{40}Ar/^{36}Ar$ around 295.5 (Nier, 1950; Steiger & Jäger, 1977). Since potentially all of the lava flows analyzed here erupted in (shallow) submarine environments, it is possible to have seawater-derived fluid inclusions in the grains. The ^{38}Ar measurement can be used as a proxy for Cl concentration, and $^{38}Ar_{(Cl)}$ can be estimated after correction for Ca and K production and atmospheric contamination (Renne et al., 2008) and is a default parameter calculated in ArArCALC v2.7.0 (Koppers, 2002). None of the samples here contain significant $^{38}Ar_{(Cl)}$ pointing to minimal effects from seawater. In addition, the K/Ca of modern seawater at ~0.95 is higher than what is observed in our samples (0.002–0.4, median 0.03). Hydrothermal fluids measured directly on Axial Seamount on the Juan de Fuca Ridge do occasionally contain Cl concentrations ~33% less than seawater (Butterfield et al., 1990). Low-Cl hydrothermal vent fluids from Axial seamount contain K/Ca of 0.4–0.6 (Butterfield et al., 1990) and thus are reasonably similar to what is observed from some of our samples. However, the lowest Cl contents of the hydrothermal fluids are still significantly higher than what we observe in the $^{40}Ar/^{39}Ar$ analyses in the clinopyroxenes, which makes fluid inclusions an unlikely source for the $^{40}Ar^*$. In addition, if seawater was the main source of ^{40}Ar in the fluid inclusions, its atmospheric composition would make it highly unlikely that the clinopyroxene ages are coeval with other comagmatic phases, such as plagioclase, hornblende, or the groundmass.

Primary or secondary melt inclusions are two other potentially K-enriched storage phases that can be hosted within clinopyroxene grains. Melt inclusions are defined as pockets of melt trapped within a crystal during growth in a magma and are commonly found within phenocrysts (Kent, 2008; Roedder, 1979; Roedder & Ribbe, 1984). Primary melt inclusions are intercrystalline packets of silicate melt that are trapped during crystal growth, while secondary inclusions represent melt infiltration along grain defects and commonly appear as flat planes of inclusions (Figures 1c and 1d). Since primary melt inclusions are typically trapped at depth, they commonly may contain excess mantle or crustal-derived $^{40}Ar/^{36}Ar$ (McDougall & Harrison, 1988). Therefore, the occasional significant increases in K/Ca with simultaneous increases in apparent age observed in some clinopyroxene heating experiments are likely associated with those excess argon bearing primary melt inclusions (Figure 2). These infrequent "bursts" of excess $^{40}Ar^*$ typically occur at the moderate to

high temperature steps in our experiments, consistent with higher-temperature breaching of the crystalline lattice, and are confined typically to a single incremental heating step. The observation that these bursts of excess $^{40}Ar^*$ occur in individual heating steps prior to the continuation of the plateau (e.g., MAL-2; Figure 2) indicates that primary melt inclusions are likely armored by the host crystal and thus not continually degassing throughout the heating experiment. More likely, temperature-dependent degradation of the crystalline structure releases trapped vapor bubbles within an individual melt inclusion (e.g., Kent, 2008). Given that each experiment consists of tens to hundreds of individual clinopyroxene crystals, significant outgassing from large vapor bearing melt inclusions is likely uncommon. However, a single (or small number of) inclusion(s) could easily alter the apparent age of a single heating step, if it carries the $^{40}Ar/^{36}Ar$ signature of up to 30,000–60,000 that is characteristic of the Earth's mantle (Graham, 2002) and much higher than the assumed 295.5 atmospheric value in $^{40}Ar/^{39}Ar$ model ages. This postulation is supported by Horton et al. (2018) who show that only a small fraction of melt inclusion bearing olivine can control the noble gas analyses for an entire separate. In the inverse isochrons, those suspect steps do plot away from the isochron and may form short arrays pointing toward significantly higher $^{40}Ar/^{36}Ar$ intercepts (e.g., the two points significantly to the left of the isochron in MAL-2; Figure 2) consistent with those higher mantle-derived argon signatures. Primary melt inclusions thus occasionally can be observed in the incremental heating experiments, but they are often not reproducible when running a second split of the same clinopyroxene separate. We conclude that the primary inclusions are uncommon in the clinopyroxenes analyzed here as evident by only a few discordant steps in the age spectra. Primary melt inclusions thus are unlikely to yield a consistent $^{40}Ar/^{39}Ar$ release pattern during incremental heating, a requirement to form an age plateau.

A more common form is secondary inclusions of silicate melt parcels trapped during the reannealing of grain defects, typically after a rapid change in magma composition during a recharge event or volatile addition/subtraction (Kent, 2008; Natland, 2003; Roedder, 1979; Roedder & Ribbe, 1984). These changes in magma composition often precede and drive the eruption of a basaltic magma (e.g., Cervantes & Wallace, 2003; O'Hara & Mathews, 1981; Tepley et al., 2000). Assuming significant degassing of the magma chamber in this (relatively long) waiting pattern and at the same time (a full) equilibration with atmospheric argon, it is possible to create trapped silicate melt inclusions that have atmospheric $^{40}Ar/^{36}Ar$. In addition, the reannealed defects are likely more easily breached during exposure to the relative low-temperature stepwise CO_2 laser heating. Argon recoil effects are relatively minor (^{39}Ar recoil length ~0.08 um; Villa, 1997) but still may play a role in effecting the age determinations. The observed K/Ca for the clinopyroxenes during low to moderate temperature heating steps are similar to the plateau range found in most nonporphyritic basaltic groundmass samples (0.1 to 1; e.g., Konrad et al., 2018; Koppers et al., 2001, 2003). Since these groundmass basalt compositions are roughly reflective of the magma chamber composition prior to eruption, the similar K/Ca of clinopyroxenes provide strong evidence that the inclusions are sourced from the host magma. However, given the consistent nature of the resulting age plateaus from this study, the breaching of reannealed grain defects must begin at relatively low temperatures and initiate high-diffusivity pathways for argon to escape from only partially armored secondary inclusions. An incremental-heating experiment carried out on amphibole grains indicated that hornblende did not structurally degrade until ~930 °C (Lee et al., 1991). Given that closure temperature for argon in clinopyroxene is greater than amphibole (e.g., Cassata et al., 2010; Lee et al., 1991), it is unlikely that clinopyroxene phenocrysts will degrade at lower than ~930 °C temperatures. This mechanism would explain why pulses of primary melt inclusion release occur at the middle- to high-temperature steps and not at the lower temperatures. It is similarly unlikely that secondary melt inclusions can be released at low temperatures, and they too are an unlikely source of $^{40}Ar^*$. More work is needed on argon diffusivity in inclusion-bearing clinopyroxenes to better understand the behavior of primary and secondary melt inclusions during incremental heating experiments.

Trace films of melt and corresponding nanomineral inclusions along defects in the clinopyroxene grains also provide a potential source for the $^{40}Ar^*$ and elevated K/Ca. Melt films along grain boundaries and defects have been observed and studied in ultramafic rocks (e.g., Drury & Fitz Gerald, 1996; Wulff-Pedersen et al., 1999), but little work has been done on individual phenocryst phases. Nanoscale silicate minerals formed within grain defects and cleavage planes may provide all the necessary components to satisfy the observed data. These films and nanomineral inclusions would have elevated K/Ca as they represent pockets of melt trapped when the magma was more evolved. The higher silicate nature of these submicroscopic phases would remain resistive to the acid leaching pretreatment of the crystals, since they are effectively

shielded by the clinopyroxene host minerals. They would become trapped during magma ascent/eruption that allows for the degassing of argon as well for an effective exchange with atmospheric gasses. Lastly, the minerals/film would already be residing within a potential high-diffusivity pathway, which allows for degassing at low- to middle-temperature incremental heating steps below ~930 °C.

In summary, in situ crystal and inclusion analyses are needed to better determine the origin of the ^{40}K and associated ^{40}Ar*. However, based on the current data set, either secondary melt inclusion bands (e.g., Kent, 2008; Natland, 2003; Roedder, 1979; Roedder & Ribbe, 1984) or nanoscale silicate inclusions along grain defects/cleavage planes are the best fit candidates. Either of these sources can provide basaltic melt K/Ca values while containing atmospheric ^{40}Ar/^{36}Ar. In addition, they satisfy the lack of excess ^{38}Ar$_{(Cl)}$ released and likely degas during relative low temperature heating.

5. Conclusions

This work further demonstrates that basaltic clinopyroxene is a viable phase for ^{40}Ar/^{39}Ar age determinations. The degassing patterns for clinopyroxene typically display long (>60%) plateaus and ages that are often concordant with more traditional coeval phases used in ^{40}Ar/^{39}Ar geochronology. Potassium and radiogenic ^{40}Ar are primarily released at lower to moderate temperature steps with corresponding K/Ca values of 0.002 to 0.4. These high K/Ca values indicate that a relatively high K phase hosted by clinopyroxene—and not the clinopyroxene itself—is the primary source of K and harbors the eruptive age information. This phase is likely either nanoscale silicate mineral inclusions present along grain defects and cleavage planes or secondary melt inclusion bands. The preferential degassing of high- and low-Ca pyroxene phases also remain a possibility for controlling the K/Ca. Clinopyroxene age dating has the potential to greatly expand our geochronological knowledge of seafloor features as it is one of the most common and alteration resistive phenocrystic phases in basalt.

Acknowledgments
We thank Jasper Konter for providing the Western Pacific Seamount Province clinopyroxene separates. Extended ^{40}Ar/^{39}Ar age determination data for these samples are available in the online EarthRef.org Digital Archive (https://earthref.org/ERDA). Fred Jourdan and an anonymous referee are thanked for reviews and discussion that improved the quality of this work.

References

Bach, W., Garrido, C. J., Paulick, H., Harvey, J., & Rosner, M. (2004). Seawater-peridotite interactions: First insights from ODP Leg 209, MAR 15°N. *Geochemistry, Geophysics, Geosystems*, *5*, Q09F26. https://doi.org/10.1029/2004GC000744

Burgess, R., Turner, G., & Harris, J. (1992). ^{40}Ar-^{39}Ar laser probe studies of clinopyroxene inclusions in eclogitic diamonds. *Geochimica et Cosmochimica Acta*, *56*(1), 389–402. https://doi.org/10.1016/0016-7037(92)90140-E

Butterfield, D. A., Massoth, G. J., McDuff, R. E., Lupton, J. E., & Lilley, M. D. (1990). Geochemistry of hydrothermal fluids from axial seamount hydrothermal emissions study vent field, Juan de Fuca Ridge: Subseafloor boiling and subsequent fluid-rock interaction. *Journal of Geophysical Research*, *95*, 12,895–12,921. https://doi.org/10.1029/JB095iB08p12895

Cassata, W. S., Renne, P. R., & Shuster, D. L. (2011). Argon diffusion in pyroxenes: Implications for thermochronometry and mantle degassing. *Earth and Planetary Science Letters*, *304*(3–4), 407–416. https://doi.org/10.1016/j.epsl.2011.02.019

Cassata, W. S., Shuster, D. L., Renne, P. R., & Weiss, B. P. (2010). Evidence for shock heating and constraints on Martian surface temperatures revealed by ^{40}Ar/^{39}Ar thermochronometry of Martian meteorites. *Geochimica et Cosmochimica Acta*, *74*(23), 6900–6920. https://doi.org/10.1016/j.gca.2010.08.027

Cervantes, P., & Wallace, P. (2003). Magma degassing and basaltic eruption styles: A case study of~ 2000 year BP Xitle volcano in central Mexico. *Journal of Volcanology and Geothermal Research*, *120*(3-4), 249–270. https://doi.org/10.1016/S0377-0273(02)00401-8

Drury, M. R., & Fitz Gerald, J. D. (1996). Grain boundary melt films in an experimentally deformed olivine-orthopyroxene rock: Implications for melt distribution in upper mantle rocks. *Geophysical Research Letters*, *23*, 701–704. https://doi.org/10.1029/96GL00702

Finlayson, V., Konter, J., Konrad, K., Koppers, A., Jackson, M., & Rooney, T. (2018). Sr–Pb–Nd–Hf isotopes and ^{40}Ar/^{39}Ar ages reveal a Hawaii–Emperor-style bend in the Rurutu hotspot. *Earth and Planetary Science Letters*, *500*, 168–179. https://doi.org/10.1016/j.epsl.2018.08.020

Graham, D. W. (2002). Noble gas isotope geochemistry of mid-ocean ridge and ocean island basalts: Characterization of mantle source reservoirs. *Reviews in Mineralogy and Geochemistry*, *47*(1), 247–317. https://doi.org/10.2138/rmg.2002.47.8

Hart, S. R., & Dunn, T. (1993). Experimental cpx/melt partitioning of 24 trace elements. *Contributions to Mineralogy and Petrology*, *113*(1), 1–8. https://doi.org/10.1007/BF00320827

Horton, F., Farley, K., & Jackson, M. (2018). Helium distributions in ocean island basalt olivines revealed by X-ray computed tomography and single-grain crushing experiments. *Geochimica et Cosmochimica Acta*. https://doi.org/10.1016/j.gca.2018.10.013

Jourdan, F., Hodges, K., Sell, B., Schaltegger, U., Wingate, M., Evins, L., et al. (2014). High-precision dating of the Kalkarindji large igneous province, Australia, and synchrony with the Early–Middle Cambrian (stage 4–5) extinction. *Geology*, *42*(6), 543–546. https://doi.org/10.1130/G35434.1

Jourdan, F., Renne, P., & Reimold, W. (2009). An appraisal of the ages of terrestrial impact structures. *Earth and Planetary Science Letters*, *286*(1–2), 1–13. https://doi.org/10.1016/j.epsl.2009.07.009

Kent, A. J. R. (2008). Melt inclusions in basaltic and related volcanic rocks. *Reviews in Mineralogy and Geochemistry*, *69*(1), 273–331. https://doi.org/10.2138/rmg.2008.69.8

Konrad, K., Koppers, A. A., Steinberger, B., Finlayson, V. A., Konter, J. G., & Jackson, M. G. (2018). On the relative motions of long-lived Pacific mantle plumes. *Nature Communications*, *9*(1), 854. https://doi.org/10.1038/s41467-018-03277-x

Konter, J. G., Staudigel, H., Blichert-Toft, J., Hanan, B., Polvé, M., Davies, G., et al. (2009). Geochemical stages at Jasper Seamount and the origin of intraplate volcanoes. *Geochemistry, Geophysics, Geosystems*, *10*, Q02001. https://doi.org/10.1029/2008GC002236

Koppers, A. A. (2002). ArArCALC—Software for $^{40}Ar/^{39}Ar$ age calculations. *Computers & Geosciences*, *28*(5), 605–619. https://doi.org/10.1016/S0098-3004(01)00095-4

Koppers, A. A., Staudigel, H., & Wijbrans, J. R. (2000). Dating crystalline groundmass separates of altered Cretaceous seamount basalts by the $^{40}Ar/^{39}Ar$ incremental heating technique. *Chemical Geology*, *166*(1-2), 139–158. https://doi.org/10.1016/S0009-2541(99)00188-6

Koppers, A. A. P., Morgan, J. P., Morgan, J. W., & Staudigel, H. (2001). Testing the fixed hotspot hypothesis using $^{40}Ar/^{39}Ar$ age progressions along seamount trails. *Earth and Planetary Science Letters*, *185*(3-4), 237–252. https://doi.org/10.1016/S0012-821X(00)00387-3

Koppers, A. A. P., Staudigel, H., Pringle, M. S., & Wijbrans, J. R. (2003). Short-lived and discontinuous intraplate volcanism in the South Pacific: Hot spots or extensional volcanism? *Geochemistry, Geophysics, Geosystems*, *4*(10), 1089. https://doi.org/10.1029/2003gc000533

Kuiper, K., Deino, A., Hilgen, F., Krijgsman, W., Renne, P., & Wijbrans, J. (2008). Synchronizing rock clocks of Earth history. *Science*, *320*(5875), 500–504. https://doi.org/10.1126/science.1154339

Kunz, J., Falter, M., & Jessberger, E. K. (1997). Shocked meteorites: Argon-40-argon-39 evidence for multiple impacts. *Meteoritics & Planetary Science*, *32*(5), 647–670. https://doi.org/10.1111/j.1945-5100.1997.tb01550.x

Lee, J., Onstott, T., Cashman, K., Cumbest, R., & Johnson, D. (1991). Incremental heating of hornblende in vacuo: Implications for $^{40}Ar/^{39}Ar$ geochronology and the interpretation of thermal histories. *Geology*, *19*(9), 872–876. https://doi.org/10.1130/0091-7613(1991)019<0872:IHOHIV>2.3.CO;2

McDougall, I., & Harrison, T. (1988). *Geochronology and thermochronology by the $^{40}Ar/^{39}Ar$ method*. New York: Oxford University Press.

Min, K., Mundil, R., Renne, P. R., & Ludwig, K. R. (2000). A test for systematic errors in $^{40}Ar/^{39}Ar$ geochronology through comparison with U/Pb analysis of a 1.1-Ga rhyolite. *Geochimica et Cosmochimica Acta*, *64*(1), 73–98. https://doi.org/10.1016/S0016-7037(99)00204-5

Miyazaki, T., Hanyu, T., Kimura, J.-I., Senda, R., Vaglarov, B. S., Chang, Q., et al. (2018). Clinopyroxene and bulk rock Sr–Nd–Hf–Pb isotope compositions of Raivavae ocean island basalts: Does clinopyroxene record early stage magma chamber processes? *Chemical Geology*, *482*, 18–31. https://doi.org/10.1016/j.chemgeo.2017.12.015

Natland, J. H. (2003). Capture of helium and other volatiles during the growth of olivine phenocrysts in picritic basalts from the Juan Fernandez Islands. *Journal of Petrology*, *44*(3), 421–456. https://doi.org/10.1093/petrology/44.3.421

Nier, A. O. (1950). A redetermination of the relative abundances of the isotopes of carbon, nitrogen, oxygen, argon, and potassium. *Physical Review*, *77*(6), 789–793. https://doi.org/10.1103/PhysRev.77.789

Nisbet, E. G., & Pearce, J. A. (1977). Clinopyroxene composition in mafic lavas from different tectonic settings. *Contributions to Mineralogy and Petrology*, *63*(2), 149–160. https://doi.org/10.1007/BF00398776

O'Hara, M., & Mathews, R. (1981). Geochemical evolution in an advancing, periodically replenished, periodically tapped, continuously fractionated magma chamber. *Journal of the Geological Society*, *138*(3), 237–277. https://doi.org/10.1144/gsjgs.138.3.0237

Reagan, M. K., Heaton, D. E., Schmitz, M. D., Pearce, J. A., Shervais, J. W., & Koppers, A. A. P. (2019). Forearc ages reveal extensive short-lived and rapid seafloor spreading following subduction initiation. *Earth and Planetary Science Letters*, *506*, 520–529. https://doi.org/10.1016/j.epsl.2018.11.020

Renne, P. R., Sharp, Z. D., & Heizler, M. T. (2008). Cl-derived argon isotope production in the CLICIT facility of OSTR reactor and the effects of the Cl-correction in $^{40}Ar/^{39}Ar$ geochronology. *Chemical Geology*, *255*(3–4), 463–466. https://doi.org/10.1016/j.chemgeo.2008.07.014

Roedder, E. (1979). Origin and significance of magmatic inclusions. *Bulletin de Mineralogie*, *102*, 487–510.

Roedder, E., & Ribbe, P. (1984). *Fluid inclusions* (Vol. 12). Washington, DC: Mineralogical Society of America.

Staudigel, H., Plank, T., White, B., & Schmincke, H. U. (1996). Geochemical fluxes during seafloor alteration of the basaltic upper oceanic crust: DSDP sites 417 and 418. Subduction top to bottom, 19–38.

Steiger, R. H., & Jäger, E. (1977). Subcommission on geochronology: Convention on the use of decay constants in geo-and cosmochronology. *Earth and Planetary Science Letters*, *36*(3), 359–362. https://doi.org/10.1016/0012-821X(77)90060-7

Tepley, F. III, Davidson, J., Tilling, R., & Arth, J. G. (2000). Magma mixing, recharge and eruption histories recorded in plagioclase phenocrysts from El Chichon Volcano, Mexico. *Journal of Petrology*, *41*(9), 1397–1411. https://doi.org/10.1093/petrology/41.9.1397

Villa, I. M. (1997). Direct determination of ^{39}Ar recoil distance. *Geochimica et Cosmochimica Acta*, *61*(3), 689–691. https://doi.org/10.1016/S0016-7037(97)00002-1

Ware, B., & Jourdan, F. (2018). $^{40}Ar/^{39}Ar$ geochronology of terrestrial pyroxene. *Geochimica et Cosmochimica Acta*, *230*, 112–136. https://doi.org/10.1016/j.gca.2018.04.002

Wulff-Pedersen, E., Neumann, E.-R., Vannucci, R., Bottazzi, P., & Ottolini, L. (1999). Silicic melts produced by reaction between peridotite and infiltrating basaltic melts: Ion probe data on glasses and minerals in veined xenoliths from La Palma, Canary Islands. *Contributions to Mineralogy and Petrology*, *137*(1–2), 59–82. https://doi.org/10.1007/s004100050582

Zhong, L.-F., Cai, G.-Q., Koppers, A. A., Xu, Y.-G., Xu, H.-H., Gao, H.-F., & Xia, B. (2018). $^{40}Ar/^{39}Ar$ dating of oceanic plagiogranite: Constraints on the initiation of seafloor spreading in the South China Sea. *Lithos*, *302*, 421–426.